LA-UR-16-26968 (Accepted Manuscript)

The role of surfaces, chemical interfaces, and disorder on plutonium incorporation in pyrochlores

Perriot, Romain Thibault
Uberuaga, Blas P.
Dholabhai, Pratik

To be published in: Physical Chemistry Chemical Physics

DOI to publisher's version: 10.1039/C6CP03543D

Permalink to record: http://permalink.lanl.gov/object/view?what=info:lanl-repo/lareport/LA-UR-16-26968

Journal Name

ARTICLE TYPE

Cite this: DOI: 10.1039/xxxxxxxxxx

The role of surfaces, chemical interfaces, and disorder on plutonium incorporation in pyrochlores

Romain Perriot,* Pratik P. Dholabhai, and Blas P. Uberuaga

Received Date
Accepted Date

DOI: 10.1039/xxxxxxxxxx

www.rsc.org/journalname

Pyrochlores, a class of complex oxides with formula $A_2B_2O_7$, are one of the candidates for nuclear waste encapsulation, due to the natural occurrence of actinide-bearing pyrochlore minerals and laboratory observations of high radiation tolerance. In this work, we use atomistic simulations to determine the role of surfaces, chemical interfaces, and cation disorder on the plutonium immobilization properties of pyrochlores as a function of pyrochlore chemistry. We find that both Pu^{3+} and Pu^{4+} segregate to the surface for the four low-index pyrochlore surfaces considered, and that the segregation energy varies with the chemistry of the compound. We also find that pyrochlore/pyrochlore bicrystals $A_2B_2O_7/A'_2B'_2O_7$ can be used to immobilize Pu^{3+} and Pu^{4+} either in the same or separate phases of the compound, depending on the chemistry of the material. Finally, we find that Pu^{4+} segregates to the disordered phase of an order/disorder bicrystal, driven by the occurence of local oxygen-rich environments. However, Pu^{3+} is weakly sensitive to the oxygen environment, and therefore only slightly favors the disordered phase. This behavior suggests that, at some concentration, Pu incorporation can destabilize the pyrochlore structure. Together, these results provide new insight into the ability of pyrochlore compounds to encapsulate Pu and suggest new considerations in the development of waste forms based on pyrochlores. In particular, the phase structure of a multi-phase pyrochlore composite can be used to independently getter decay products based on their valence and size.

1 Introduction

The treatment of nuclear waste in the energy cycle poses a critical problem, as long-lived fission products and actinides remain active for thousands of years[1]. One approach to treating that waste is to encapsulate it in a matrix made of complex oxide materials, such as perovskites, zirconolites, or pyrochlores[2–6]. Pyrochlores, of formula $A_2B_2O_7$, in particular are a promising candidate for waste immobilization, due their high tolerance to radiation[7–9], and the natural occurence of actinides-bearing pyrochlores[2,6,10]. These natural analogues suggest that pyrochlores can accomodate actinide species for extremely long times and have spurred the great deal of laboratory work that has occurred during the last four decades. Because of their natural stability, pyrochlore phases are a major component of Synroc-F[11], a version of a composite material incorporating several oxides, each of which is targeting the immobilization of a specific element[12].

Early experimental efforts focused on titanate pyrochlores, as the natural minerals generally contain Ti[13], which were found to amorphize easily[14–17]. Thus, the focus shifted to zirconate pyrochlores, which are much more tolerant to radiation[7,9,18,19]. Investigation of Pu in solution in $La_2Zr_2O_7$ showed that plutonium can take either the 3+ or 4+ valence states in this material, with Pu^{3+} always occupiying the A (La^{3+}) site, and Pu^{4+} substituting on either the A (La^{3+}) or B (Zr^{4+}) site[20–22]. Those results were complemented by computational studies that determined the defect chemistry and solution energy of Pu^{3+} and Pu^{4+} in $Gd_2Zr_2O_7$[23]. A more comprehensive study[24] that looked at a wide range of pyrochlore compounds found that the chemical composition of the material affects the defect chemistry, just like it dictates many properties in pyrochlores including tolerance to radiation[7,8], structure[25], ionic conductivity[26,27], and defect stability[28]. Although the work of Cleave and coworkers[24] elucidates crucial solution mechanisms as a function of the material's chemical composition, the effect of the chemistry on the ability of solutes to redistribute in a complex material, for instance the behavior of Pu at surfaces, remains to be determined. Moreover, while complete amorphization was shown to drastically alter the immobilization properties of pyrochlore matrices[29,30], the influence of cation disorder, which is the dominant radiation-tolerant mechanism for radiation-tolerant compositions, has been overlooked. In addition, the promising properties of composite materials motivate the investigation of chemical interfacial effects in

Materials Science and Technology Division, Los Alamos National Laboratory P.O. Box 1663, Los Alamos, NM 87545
* Corresponding author. E-mail: rperriot@lanl.gov

multiphase materials. As such, pyrochlore/pyrochlore bicrystals are a simple model of composites more generally, and may offer further insights into immobilization strategies.

In this work, we used molecular dynamics simulations to investigate the segregation of Pu^{3+} and Pu^{4+} to the surface of four low-index pyrochlore surfaces, as well as to chemical interfaces in $A_2B_2O_7/A'_2B'_2O_7$ pyrochlore/pyrochlore bicrystals. We found that Pu segregates to the surface of pyrochlore crystals for all surfaces considered. We also found that pyrochlore/pyrochlore bicrystals can be used to immobilize Pu waste, and that the material can be designed such that Pu^{3+} and Pu^{4+} segregate to the same or different phases (phases are to be understood as different chemical composition or disorder level in this paper). Finally, we considered the effect of radiation on the immobilization properties of pyrochlores by determining the segregation tendencies of Pu in a mixed order/disorder system. The role of disorder is critical to the design of an efficient encapsulation matrix, since radiation due to Pu α–decay will inevitably occur and alter the structure and properties of the material over time.

2 Methodology

2.1 Defect chemistry of Pu in pyrochlore

The solution reactions of Pu^{3+} and Pu^{4+} in pyrochlores, through Pu_2O_3 and PuO_2, respectively, were elucidated by the means of empirical potentials by Cleave and coworkers[24]. Although many solution reactions are possible, notably through creation of charge-compensating oxygen or cation interstitials and vacancies, it was found that the most favorable reaction for Pu^{3+} incorporation is the simple substition reaction $Pu^{3+} \leftrightarrow A^{3+}$, in agreement with experimental findings[22], for the whole range of pyrochlore compounds $A_2B_2O_7$ considered:

$$Pu_2O_3 + 2A_A{}^{\times} \rightarrow A_2O_3 + 2Pu_A^{\times}, \quad (1)$$

Henceforth, the Kröger-Vink notation[31] is adopted: $A_A{}^{\times}$ and $B_B{}^{\times}$ denote the defect-free pyrochlore compounds; $Pu_A{}^{\times}$ and $Pu_B{}^{\times}$ the compound with one charge-neutral $Pu^{3+} \leftrightarrow A^{3+}$ and $Pu^{4+} \leftrightarrow B^{4+}$ substitution, respectively; $Pu_A^{\bullet}$ the substitution $Pu^{4+} \leftrightarrow A^{3+}$, which has charge +1; O_i'' to an oxygen interstitial, with charge -2. The charge and stoichiometry-conserving substitution mechanism for Pu^{4+}, $Pu^{4+} \leftrightarrow B^{4+}$,

$$PuO_2 + 2B_B^{\times} \rightarrow BO_2 + 2Pu_B^{\times}, \quad (2)$$

is also the preferred reaction for most of the studied pyrochlore chemistries. In rare occurences, more complex mechanisms involving oxygen interstitials O_i, antisites A_B, and incorporation of Pu^{4+} on both the A and B sites, are favored over reaction (2). Examples of when other reactions are preferred include in the $A_2Sn_2O_7$ series, for $A = Gd \rightarrow Lu$, the $A_2Zr_2O_7$ series, for $A = Sm \rightarrow Gd$, and $Gd_2Pb_2O_7$ (no A cation smaller than Gd was considered for Pb and Zr). For these compositions, the preferred reactions are:

$$4PuO_2 + 4A_A^{\times} + 2B_B^{\times} \rightarrow 4Pu_A^{\bullet} + 2A'_B + O_i'' + A_2B_2O_7, \quad (3)$$

$$4PuO_2 + 2A_A^{\times} + 2B_B^{\times} \rightarrow 2Pu_A^{\bullet} + 2Pu_B^{\times} + O_i'' + A_2B_2O_7, \quad (4)$$

with Eq. (3) only favored in stannates for $A = Er, Yb, Lu$. In addition to being less common, the difference in energy between these complex mechanisms and the substitution mechanisms is small (<0.2eV)[24]. For this reason and for simplicity, only the direct substitution mechanisms, Eqs. (1) and (2), were considered in the present work.

Table 1 Parameterization of the Buckingham potential used in this study

Interaction	A (eV)	ρ (Å)	C (eV/Å^6)	Ref.
O^{2-}–O^{2-}	9547.96	0.2192	32.0	35
La^{3+}–O^{2-}	2088.89	0.3460	23.25	35
Sm^{3+}–O^{2-}	1944.44	0.3414	21.49	35
Gd^{3+}–O^{2-}	1885.75	0.3399	20.34	35
Tb^{3+}–O^{2-}	1818.0	0.33845	14.33	36
Y^{3+}–O^{2-}	1766.40	0.33849	19.43	35
Ho^{3+}–O^{2-}	1726.29	0.33776	10.76	36
Yb^{3+}–O^{2-}	1649.80	0.3386	16.57	35
Lu^{3+}–O^{2-}	1618.8	0.33849	19.27	35
Ti^{4+}–O^{2-}	2131.04	0.3038	0.0	35
Mo^{4+}–O^{2-}	1223.97	0.3470	0.0	35
Hf^{4+}–O^{2-}	1492.60	0.3478	7.6	37
Zr^{4+}–O^{2-}	1502.11	0.3477	5.1	35
Pb^{4+}–O^{2-}	1640.34	0.3507	19.5	35
Pu^{3+}–O^{2-}	1150.745	0.3743	11.48	24
Pu^{4+}–O^{2-}	1762.840	0.3542	12.10	24

2.2 Potential model

All the results presented in this paper were obtained by the means of empirical potential calculations, utilizing the Buckingham potential form for short-range interatomic interactions:

$$V(r) = A \times \exp\left(-\frac{r}{\rho}\right) + \frac{C}{r^6}, \quad (5)$$

where A, C, and ρ are adjustable parameters. Formal charges are adopted, and the Coulomb interaction is calculated via the Ewald sum technique. The parameterization of the various A^{3+}–O^{2-}, B^{4+}–O^{2-}, as well as Pu^{3+}–O^{2-} and Pu^{4+}–O^{2-} interactions, is summarized in table 1. The set was derived by the Grimes group at Imperial College, and fitted against the same O^{2-}–O^{2-} parameterization, ensuring consistency of the set as a whole. The LAMMPS code[32] was used to perform the calculations.

Although the Buckingham form is rather simple, forbidding notably any charge transfer between ions, it has been widely used to study the properties of complex oxides, and has been repeatedly demonstrated to reveal physically meaningful trends in these types of materials, in agreement with experimental[7,8] and density functional theory[33,34] results.

2.3 Pyrochlore surfaces

In order to look at the segregation of Pu^{3+} and Pu^{4+} to pyrochlore surfaces, we consider four low-index orientations: (100), (110), (111), and (112). Due to the structural complexity of pyrochlores, the construction of dipole-free surfaces respecting the pyrochlore stoichiometry is non-trivial, and described elsewhere[38]. The constructed surfaces were annealed and relaxed, and we used the lowest energy structure found for each orientation (labelled as (100)-a, (110)-a_1, (111)-c_1, and (112)-b_2, respectively in Ref. 38). Independently of the chemistry, it was found that the surface energies rank, from highest to lowest: $(100) > (111) > (112) > (110)$[38]. Each A^{3+} atom was replaced with a Pu^{3+} atom, and the whole structure relaxed to obtain the energy of the Pu^{3+}-"doped" structure as a function of position of the Pu ion. The robust steepest descent method was used for the relaxation algorithm. The same procedure was used for Pu^{4+}, in which Pu^{4+} was substituted on B^{4+} sites.

2.4 Pyrochlore/pyrochlore bicrystals

We constructed pyrochlore/pyrochlore bicrystals by juxtaposing two $4 \times 4 \times 4$ unit cells, creating a $4 \times 4 \times 8$ supercell of $A_2B_2O_7/A'_2B'_2O_7$, with periodic boundary conditions (PBC) in all three directions and a (100)/(100) interface. This construction ensures a stoichiometric simulation cell. Further, for simplicity we assume a fully coherent interface. We considered a set of A/A' and B/B' chemistries, covering an extensive range of ionic radii from 0.977 (Lu^{3+}) to 1.160 Å (La^{3+}) for the A site, and 0.605 (Ti^{4+}) to 0.775 Å (Pb^{4+}) for the B site, see Fig. 1. The ionic radius of Pu^{3+} for an eight-fold oxygen coordination (CN=VIII) has not been reported, however it can be estimated based on the the increase in ionic radii of other 3+ cations from CN=VI to CN=VIII (0.12–0.13 Å[39]), and an increase of the radius of actinides compared to lanthanides in the same column by 0.02–0.05 Å. We therefore estimate the radius of Pu^{3+} to be about 1.10–1.13 Å (in between Sm^{3+} and La^{3+}), an estimation further justified in Sec. 3.2. In total, about a hundred different bicrystals were considered. It is to be noted that some of the compounds studied are experimentally observed to adopt structures other than pyrochlore[25]: disordered fluorite, δ-phase, monoclinic pyrochlore, or combinations of several forms. However, the pyrochlore form is at least metastable with the Buckingham potential for these chemistries, and such compounds are here considered as limiting cases. Sn^{4+}, which possesses a more covalent character than other B chemistries, was ignored due to the inability of Buckingham potentials to reproduce this feature. Similarly, Ru which is known to take either the 3+ or 4+ valence, was excluded from the set of chemistries considered in this work.

The lattice mismatch was accomodated by relaxing the box dimensions as well as the atomic positions before the substitution. However, for some cases the effect of strain was also investigated by scaling the dimensions of the compound with the smallest lattice constant to the size of the largest compound. As was done with the surfaces, substitutions $Pu^{3+} \leftrightarrow A$ and $Pu^{4+} \leftrightarrow B$ were performed at each atomic site, and the whole sample relaxed.

2.5 Pyrochlore/defect fluorite bicrystal

Pyrochlores ($A_2B_2O_7$) are a superstructure of the parent fluorite structure (B_4O_8), distinct from the latter by having two cation sublattices and a vacant oxygen site. When the cations are randomly exchanged, the oxygen quickly disorder as well[40]; the pyrochlore is fully disordered and can therefore be described as a defect fluorite structure, defective in the sense that one eighth of the oxygens are missing and the two cation species are not equivalent. A transformation from ordered pyrochlore to defect fluorite is a key consequence of irradiation on many pyrochlore chemistries[8,41,42] and thus understanding how disorder influences Pu distributions is critical. A order-pyrochlore/disorder-fluorite mixed system was constructed by juxtaposing two $4 \times 4 \times 8$ unit cells samples, one where the cations are ordered (i.e. in the pyrochlore structure), the other where the cations are randomly assigned on each site (i.e. defect fluorite). The resulting sample has dimensions $\sim 2 \times 2 \times 8$ nm^3 (4816 atoms), and a (100)/(100) fully coherent interface. In a disordered pyrochlore, the oxygens are no longer tied to a particular cation site[43]. A consequence of this flexibility of the oxygen sublattice is that there is no dominant ground state for a disordered pyrochlore, instead, multiple states almost degenerate in energy are possible. In order to account for this statistical distribution of states, the following procedure was applied: the as-constructed structures were minimized by relaxing both the atomic positions and the box dimensions, and subsequently equilibrated during 50 ps at 3000 K. After the initial equilibration, five independent 10 ps runs were performed at the same temperature, the resulting structures quenched to 0K during 20 ps runs, and finally the atomic positions relaxed. This procedure yielded five independent structures, all representative of the order/disorder material, in which the oxygen distributions within the disordered phase are different. The Pu substitution was then performed on the minimized structures.

Although it was recently revealed that short-range order exists in disordered pyrochlores[44], we expect that fully random cation arrangements, such as those used here, accurately capture the behavior of these materials given that, for instance, random defect fluorite structures are able to reproduce the order–disorder critical temperature of pyrochlores[45,46].

3 Results

3.1 Pu segregation at pyrochlore surfaces

The atomic structures for the four low-index surfaces considered in this work are shown in Fig. 2. Because the surfaces were constructed using a slab model, for each surface slab there are two surface structures in the simulation cell. For each surface orientation, the results for Pu^{3+} and Pu^{4+} segregation are shown in Fig. 3 for $Gd_2Ti_2O_7$ (GTO) and $Gd_2Zr_2O_7$ (GZO) pyrochlores, two chemistries known to exhibit significantly different behavior – notably in disordering tendencies[7,45]. For all surfaces and both chemistries, it can be seen that the solute (Pu) always segregates to the surface of the material, which is not surprising as similar behavior has been predicted and/or experimentally observed for solutes, impurites, or dopants in many other oxides: $MgAl_2O_4$[47], UO_2[48], CeO_2[49], SnO_2[50], ZrO_2[51], MgO[52,53],

Al_2O_3 [54,55] and Cr_2O_3 [51,56].

Figure 4 summarizes the resulting segregation energies, using the lowest energy at each of the two surfaces in a given slab to compute the segregation energy. Because annealing may render slightly different atomic arrangements at the two surfaces in a given slab, different segregation energies may be observed at each surface. If this is the case, the average value is reported, and the difference reflected by error bars. The value for the (110) surface, which was not changed after annealing [38], accordingly has no error bar; in other words, it exhibits a fully symmetric energy profile and identical energies on both surfaces. From Fig. 4, trends common to all surfaces are extracted: the segregation energy is higher for Pu^{4+} than Pu^{3+}, and higher for GTO than GZO. In order to further investigate the role of chemistry on the segregation energy, two additional compositions with a smaller A cation, $Lu_2Ti_2O_7$ (LTO) and $Lu_2Zr_2O_7$ (LZO), were considered. The segregation energies for these compounds are also summarized in Fig. 4, confirming both trends: $E_{seg}[Pu^{3+}] < E_{seg}[Pu^{4+}]$ and the higher segregation energy to titanates surfaces as compared to zirconate surfaces. For each surface, and regardless of the Pu valence, the highest segregation energies are observed for LTO then GTO. In contrast, LZO and GZO exhibit similar segregation energies, and the order alternates depending on the surface. The higher surface energy of titanates [38] offers an enhanced opportunity for stabilization, though segregation energies do not always correlate with surface energies [47]. It is to be noted that the surface exhibiting the weakest Pu^{3+} segregation ((110) in GTO) is not the weakest for Pu^{4+} substitution ((112) in this case). The surface with the highest energy ((100) before Pu substitution) does however exhibit consistently higher segregation energies. More than the differences in surface energy, the higher segregation energy for titanates over zirconates, and Lu over Gd, can be explained by the ionic radius difference between the species. Pu^{4+} has a larger ionic radius than both Zr and Ti (see Fig. 1), such that the atom will preferentially sit at the surface, where more open volume is available; in addition, the larger Zr ionic bulk site will accomodate Pu^{4+} with more ease than Ti, yielding a lower segregation energy for the zirconates. A similar explanation holds for Pu^{3+}, however the smaller difference in ionic radii between Pu^{3+} and the other A cations means a reduced mismatch in the bulk and, as a consequence, a lower segregation energy. This explains why the chemistry of the A-site, which did not affect the surface stability [38], however has a significant impact on the segregation energy.

3.2 Pu segregation in pyrochlore/pyrochlore bicrystals

The role of chemical interfaces was examined by creating pyrochlore bicrystals $A_2B_2O_7/A'_2B'_2O_7$, considering a wide range of ionic radii for the A and B chemistries (see Fig. 1). An example result is shown in Fig. 5, comparing the segregation location and energy of Pu^{3+} and Pu^{4+} in $La_2Zr_2O_7/Lu_2Ti_2O_7$ (Fig 5-a) and $La_2Ti_2O_7/Lu_2Zr_2O_7$ (Fig 5-b). (For simplicity, in the remainder of the paper, the bicrystals will be labelled according the the cation species only, i.e. LaZr/LuTi, LaTi/LuZr.) In both bicrystals, Pu^{3+} segregates to the La phase, while Pu^{4+} goes to the Zr phase, in both cases the phase with the larger cation of the same valence. Interestingly, the segregation energies are similar for each of Pu^{3+} and Pu^{4+} in LaZr/LuTi and LaTi/LuZr, revealing that the B-chemistry is relatively irrelevant in determining Pu^{3+} substitution, and similarly Pu^{4+} is not sensitive to the A cation chemistry. We also observed that the segregation energy of Pu^{4+} is much higher than for Pu^{3+} ($\sim$ 10 eV *vs.* $\sim$ 4 eV).

To further assess the role of chemistry on the segregation location and energy, we surveyed a range of chemistries on both the A site (AZr/A'Ti (Fig. 6)) and the B site (LaB/LuB' (Fig. 7)). From Fig. 6, where the A/A' chemistry was chosen to systematically increase the ionic radius difference between A and A' ($\Delta r_A = r_A - r_{A'}$ =0.0 Å for La/La, 0.115 Å for La/Lu), the following observations can be made: i) the solute always segregates to the phase bearing the larger ion of same valence; ii) the segregation energy of Pu^{3+} increases with Δr_A; and iii) the segregation energy of Pu^{4+} is mostly insensitive to Δr_A. In addition,we found the the segregation energy of Pu^{3+} in LuZr/LuTi (not shown here) is small ($\sim$ 0.25 eV) similarly to LaZr/LaTi. Accordingly, results for LaB/LuB' (Fig. 7) show: i) the solute always segregates to the phase bearing the larger ion of same valence; ii) the segregation energy of Pu^{4+} increases with $\Delta r_B = r_B - r_{B'}$; and iii) the segregation energy of Pu^{3+} is mostly insensitive to Δr_B, with an energy spread similar as for Pu^{4+} in AZr/A'Ti.

By comparing the ionic radii of Pu^{4+} with the host atoms (see Fig. 1), it is clear why the solute always segregates to the phase containing the larger ion. The large Pu^{4+} will be more easily accomodated in the position of a large cation, while its substitution with a smaller cation will result in larger distortions of its environment to accomodate its size. A calculation of Pu^{4+} segregation in LaZr/LuTi where the lattice constant was fixed to that of LaZr (i.e. LuTi strained) showed a 7% reduction of the segregation energy compared to a fully relaxed cell, adding to the demonstration that the small size of the B site makes it highly unfavorable. The size argument holds for Pu^{3+} as well, however its size is closer to that of the host 3+ ions, implying a reduced strain and, accordingly, a smaller driving force to segregate to one chemistry over another. As an aside, the Pu^{3+} substitution induces a deformation of the local environment away from the ion for all chemistries, except for La^{3+}, where the local environment is slightly pulled towards the ion. This observation validates the assumption made in the methods section (Sec. 2.4) that the radius of Pu^{3+} with an eightfold oxygen coordination is in-between La and Sm.

The three observations made above – segregation of the solute to the phase bearing the larger ion, increase of the segregation energy with difference in corresponding (i.e. with same valence) ionic radius, weak sensitivity to other cation in the composition – were verified for 107 pyrochlore bicrystal compositions, with A/A'=La→Lu in the lanthanide series, and B/B'=Pb→Ti post-transition and transition metals. We also found that the data can be fit to a linear function of the ionic radius difference (regardless of the actual chemistry) and provide accurate predictions of the segregation tendencies in these bicrystals, see Fig. 8.

It is to be noted that these results were obtained by assuming a chemical potential $\mu_0 = 0$; in other words an ion of the material is taken away to infinitity, from where Pu is obtained (though, since the chemical potential of Pu identically cancels when comparing

reactions, this really defines the chemical potential of the cations in the pyrochlore phase). The corresponding reactions thus are:

$$Pu_B^{\times} + B_{gas}^{ion} + B'^{\times}_{B'} \rightarrow Pu_{B'}^{\times} + B'^{\,ion}_{gas} + B_B^{\times}, \quad (6)$$

$$Pu_A^{\times} + A_{gas}^{ion} + A'^{\times}_{A'} \rightarrow Pu_{A'}^{\times} + A'^{\,ion}_{gas} + A_A^{\times}, \quad (7)$$

for Pu^{4+} and Pu^{3+} incorporation, respectively. In these reactions, the presence of the second pyrochlore phase in the bicrystal is implied.

However this choice of chemical potential is not unique; for example, another possibility would be to use the oxide and sesquioxide phases of Pu and the element it replaces, similar to the approach taken by Cleave and coworker's work[24]. To compare Pu substitution into two different phases of pyrochlore, the reactions corresponding to this second chemical potential are:

$$Pu_B^{\times} + BO_2 + B'^{\times}_{B'} \rightarrow Pu_{B'}^{\times} + B'O_2 + B_B^{\times}, \quad (8)$$

$$Pu_A^{\times} + \frac{1}{2}A_2O_3 + A'^{\times}_{A'} \rightarrow Pu_{A'}^{\times} + \frac{1}{2}A'_2O_3 + A_A^{\times}, \quad (9)$$

for Pu^{4+} and Pu^{3+} incorporation, respectively.

To understand how the trends presented in Figs. 6–8 depend on the choice of chemical potential, we used this second approach to calculate the preference of Pu for one or the other component of the bicrystal (though, in this case, we considered each phase in separate supercells, not together in one bicrystal structure with an interface) with a limited set of compositions A_2Zr_2O7/A'_2Ti_2O7, with A/A' and A'/A= La/Lu, La/Tb, Sm/Tb, Gd/Y, La/La, Lu/Lu, for a total of 10 compositions. Thus, $r_A - r'_A$ was allowed to vary from -0.184 to +0.184. Comparisons of the results obtained using the two different chemical potential reference states for this set of compositions are presented in Figs. 9 and 10. We find that the trend that Pu^{4+} segregates to the phase with the larger 4+ cation remains regardless of the chemical potential. Further, the magnitude of the differences in segregation energy caused by the A/A' chemistry is similar with both chemical potentials. The case of Pu^{3+} is more complicated. With the first chemical potential, Pu^{3+} segregation is directly related to the size of the A and A' cations. However, for the second definition, Pu^{3+} occasionally prefers to go to the phase with the smaller 3+ cation. In fact, it appears that Pu^{3+} favors the Zr-bearing phase for all the compositions, implying that the B chemistry plays a role, in contrast with results obtained with the first chemical potential. Further, the energy differences are much smaller with the second chemical potential than the first. Thus, while there are still strong differences in segregation depending on the A chemistry of the pyrochlore, the dependencies on ionic size of the A cations is more complicated for the second chemical potential.

3.3 Effect of disorder

One of the attractive properties of pyrochlores for nuclear waste encapsulation is their resistance to amorphization, which is linked to their ability to produce cation disorder in the form of antisites[7]. Such disorder will notably be induced by the α-decay of Pu in the material[10,57,58], and making it therefore critical to understand the effect of disorder on the Pu segregation properties of pyrochlores. We examined Pu segregation in GTO and GZO order/disorder bicrystals, constructed as described in Sec. 2.5, allowing us to investigate Pu segregation behavior within a disordered material, as well as the possible effect of the order/disorder interface. The results are summarized in Fig. 11, where the top panel shows the atomic structure of the bicrystals. The disordered region is clearly recognizable by the absence of a clear cation arrangement pattern, as opposed to the ordered region, and also by the distortion of the oxygen sublattice. Those distortions are the signature of the oxygens not being strongly tied to the cation sublattice, and the source for pyrochlore's high ionic conductivity[43]. As discussed earlier, the flexibility of the oxygen sublattice led us to perform Pu substitution on five different structures, all representative of the order/disorder system with differing oxygen distributions.

For both the GTO (Fig. 11-a) and GZO (Fig. 11-b) systems, the Pu^{3+} and Pu^{4+} substitution energies are constant in the bulk of the ordered region, which is consistent with all sites being equivalent in the ordered pyrochlore structure, and this energy was used as a reference. By constrast, the energies are widely spread in the disordered material, reflecting the many unique environments (both in terms of oxygen and cations) in this region. As could be anticipated, some sites are favorable to Pu substitution, while some are not. in GTO, the distribution of energies about the zero of energy for Pu^{3+} is very symmetric, while those for Pu^{4+} are largely negative. The total spread of the site energies is also much smaller for Pu^{3+} (+0.4 to -0.4 eV), than Pu^{4+} (+2 to -5 eV). Thus we can predict significant segregation of Pu^{4+} to the disordered phase in GTO, while the effect will be less pronounced for Pu^{3+}. This is even more dramatic for the GZO system (Fig. 11-b), in which Pu^{3+} appears mostly to prefer the ordered environment, although some isolated sites in the disordered region do have negative energy. The energy difference amplitude is also smaller than for GTO (+0.2 to -0.2 eV). However, the Pu^{4+} incorporation is almost always favorable in the disordered region (negative energies), even though the effect is again weaker than in GTO (-2 eV at most).

In Fig. 12, a closer look at the substitution sites is provided for the Pu^{4+} case. In Fig. 12-a, a clear correlation between the substitution energy on a given site and the site's oxygen coordination is observed: Pu^{4+} prefers an oxygen-rich environment, which is consistent with the observation that substitution on the *A*-site (relatively oxygen-rich in ordered pyrochlores) is possible in addition to *B*-site substitution[24]. This observation also explains why Pu^{4+} strongly prefers the disordered region, as opposed to the ordered region where each B^{4+} cation is surrounded by 6 oxygens only. A correlation can also be found between the cation environment (i.e. *A* or *B*-rich) and the substitution energy (see Fig. 12-b), where *B*-rich environments exhibit a lower segregation energy. However, this correlation is most likely due to the indirect effect that *B*-rich environments are also O-rich, as seen in Fig. 12-c. The dip in the center of the figure reflects the contribution of the ordered region, where all *B* substitution sites are surrounded

by only 6 oxygens. The relation between oxygen coordination and cation environment is clearly pronounced, leading us to the conclusion that the cation environment is only indirectly acting on the site substitution energy by increasing or lowering the local oxygen coordination.

The opposite conclusions are drawn for Pu^{3+} substitution: an *A*-rich environment results in a lower oxygen coordination (Fig. 13-c), and thus a lower substitution energy (Fig. 13-b), though again the two measures of the local environment are not independent. However, the lower coordination seems only slightly preferred by Pu^{3+}, and the energy differences are much smaller than for Pu^{4+}. In particular, Pu^{3+} in GZO has the same average energy whether it is six- or eight-fold coordinated with oxygen (Fig. 13-a).

4 Discussion

Our results show that, unsurprisingly, Pu, regardless of charge state, will segregate to free surfaces. In the framework of nuclear waste encapsulation, the segregation of solutes to the surface constitute an issue that should be mitigated. If the surfaces become Pu rich, then Pu is more likely to be exposed to the environment. It must be pointed out that the most stable pyrochlore surface (110), which should therefore be the dominant facet of realistic crystal, is also the one with the lowest segregation energy, somewhat mitigating the issue. However, the relatively low segregation energy of Pu to surfaces compared to what can be achieved in the bicrystals can provide one path to mitigate surface effects (this point will be discussed further below). The choice of the chemistry also plays a critical role to further reduce the segregation strength of the material, as we showed that zirconates for instance have lower surface segregation energy than titanates.

We also show that pyrochlore bicrystals offer very interesting opportunities to immobilize Pu^{3+} and Pu^{4+}. Our results reveal that the chemistry of bicrystals can be chosen to increase the segregation energy of the solute, as well as control where they segregate to, allowing for the immobilization of Pu^{3+} or Pu^{4+} either to the same phase or to separate phases. The absence of noticeable interfacial effects, as opposed for instance to what was observed at perovskite/fluorite interfaces[59], is a valuable property, ensuring notably that the concentration of solute in the preferred phase is dominated by the segregation energy between the two phases. It is to be noted, however, that the interfaces built in this work are fully coherent. The behavior of more complex interfaces, involving notably stress-releasing misfit dislocations, remains to be determined, and is beyond the scope of this paper.

Also of critical importance is the radiation tolerance of the material, necessary to maintain its integrity, and also driven by its composition. The preference for segregation to the defect-fluorite phase in the case of Pu^{4+} is thus an advantage, as irradiation conditions will unavoidably induce cation disorder. Specifically, the strong prefence of Pu^{4+} for disordered environments can lead to a stronger encapsulation inside disordered tracks. A potential drawback would be a higher leeching tendency of the disordered phase, as was observed after amorphization[29,30], however experimental studies on $Nd_2Zr_2O_7$ pyrochlores, where the Nd content was varied to produce pyrochlore→defect fluorite structures[60], showed that the dissolution rate of the disordered phase was not faster than the ordered phase. Although more than one parameter was varied during those experiments, namely disorder and stoichiometry, these observations are encouraging regarding the stability of disordered pyrochlores. Regarding Pu^{3+}, we showed that many favorable sites are available in GTO, however in GZO it will most likely be drawn to the ordered region, favored entropically by the higher number of sites with similar energy. Lastly, the exposed relation between oxygen environment and substitution energy offers an additional way to enhance Pu encapsulation, through oxygen-doping, usually achieved by aliovalent cation doping or changing the stoichiometry of the compound.

It is also worth noting that the incorporation of Pu cations can stabilize the disordered phase of pyrochlores, unless precipitation or phase segregation first occurs. As a limiting case, we used special quasirandom structures (SQS[61]) to obtain a representative disordered structure and calculate the disordering energy of Pu-based compounds, an approach previously used to determine the disordering tendencies of pyrochlores as a function of chemistry[45]. We found that both $Pu_2Zr_2O_7$ and $Pu_2Ti_2O_7$ – with Pu as Pu^{3+} – have negative disordering energies (-4.2 and -5.1 eV, respectively); in other words the disordered fluorite structure is favored over the pyrochlore structure for these compounds. $Gd_2Pu_2O_7$ – with Pu as Pu^{4+} – has a disordering energy of only 0.1 eV. For comparison, the disordering energy obtained for the series $Gd_2B_2O_7$ with B=Pb, Zr, Hf, Sn, Mo, Ti (also with empirical potentials) goes from 1.2 to 3.3 eV[38]. These results indicate that Pu, upon incorporation into pyrochlore, can destabilize the pyrochlore structure, however we have not determined at which level this will occur. This has important consequences for the use of these materials as waste forms and the radiation stability of these compounds.

More generally, our results indicate that the phase structure of a pyrochlore composite can be used to control the distributions of encapsulated Pu to a high degree. The phases themselves, whether via chemistry or disorder, effectively getter the Pu and thus chemistry and disorder can be used as design parameters to enhance Pu encapsulation in the composite. For example, as alluded to above, one can imagine a core-shell structure in which the interior is a phase that strongly getters Pu while the shell is a chemistry of pyrochlore that does not, protecting the surface from becoming Pu rich and thus effectively mitigating the surface segregation issue, see Fig. 14. Further, the structure could be adapted to effectively segregate decay products of different size or valence charge. U^{4+} for instance, with a chemistry close to that of Pu^{4+}, could be easily segregated form Pu^{3+}. Similar concepts, in which multiphase ceramic composites are envisioned to getter different species either during burn-up in nuclear fuel[62,63] or in the fabrication of nuclear waste forms[11,12], have been proposed in the past. Our work shows that even keeping the phase structure constant and only modifying the chemistry of the different phases can lead to composite structures that can accomplish these goals. Past work has also shown how the phase structure of a composite can be used to mitigate irradiation-induced defect evolution, by using the phases themselves as sinks for defects[64,65], similar to the current results for Pu segregation. Together, this body of work

highlights the idea of using the phase structure of a composite to design materials with improved performance for nuclear energy applications.

5 Conclusions

To conclude, we used atomistic simulations to provide insight into the properties of pyrochlore surfaces and bicrystal structure for Pu immobilization. It was found that the defects weakly segregate to the pyrochlore free surface, for each of the considered surfaces, and that the segregation strength varies with the particular surface and material chemistry. We also observed that, in pyrochlore bicrystals $A_2B_2O_7/A'_2B'_2O_7$, the segregation energy and the segregation phase are dictated by the chemistry of the material, allowing for the segregation of Pu^{3+} and Pu^{4+} to common or separate pyrochlore phases. Finally, we found that a disordered pyrochlore phase offers favorable segregation sites for Pu, ensuring that the material will remain capable of immobilizing defects in an irradiated environment. This last result also suggests that the incorporation of Pu can be enhanced by oxygen-doping. Together with the established knowledge of the chemistry effect on the radiation tolerance of pyrochlores, these results provide new opportunities for the design of efficient and tailored waste encapsulation matrices.

Acknowledgements

The authors are grateful to Chris Stanek, Sarah Finkeldei and Felix Brandt for insightful discussions. This work was supported by the U.S. Department of Energy, Office of Science, Basic Energy Sciences, Materials Sciences and Engineering Division under award 2013LANL8400. This research used ressources provided by the LANL Institutional Computing Program. Los Alamos National Laboratory, an affirmative action equal opportunity employer, is operated by Los Alamos National Security, LLC, for the National Nuclear Security Administration of the U.S. DOE under contract DE-AC52- 06NA25396.

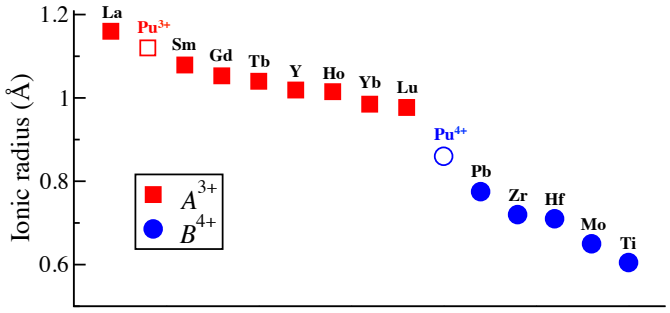

Fig. 1 Ionic radii for the chemical elements considered in the various pyrochlore bicrystals. Data taken from Ref. 39, with coordination number CN=VIII for A^{3+}, and CN=VI for B^{4+}, except Pu^{3+} (since CN=VIII is not available for Pu^{3+}, the ionic radius was estimated, see text). The elements are ordered by size along the x-axis.

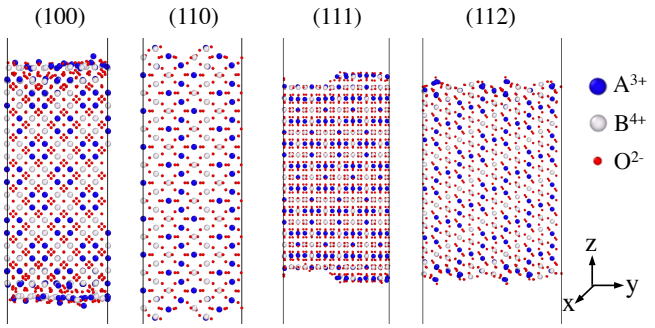

Fig. 2 The four low-index surfaces of pyrochlore considered in this work. The construction of the stoichiometric and dipole-free slabs is discussed in Ref. 38. We here used the stabilized annealed structures, which were lowest in energy and which explains why the slabs are not perfectly symmetric.

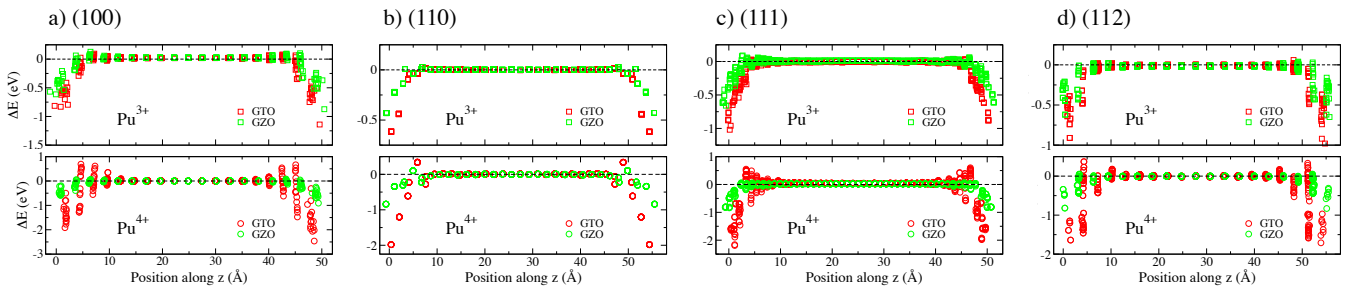

Fig. 3 Energy profiles of Pu^{3+} (top) and Pu^{4+} (bottom) near the (100) (a), (110) (b), (111) (c), and (112) (d) pyrochlore surfaces. In each plot, the zero of energy was shifted such that zero corresponds to the incorporation energy in the bulk and negative (positive) energies correspond to sites that are more (less) favorable than in the bulk.

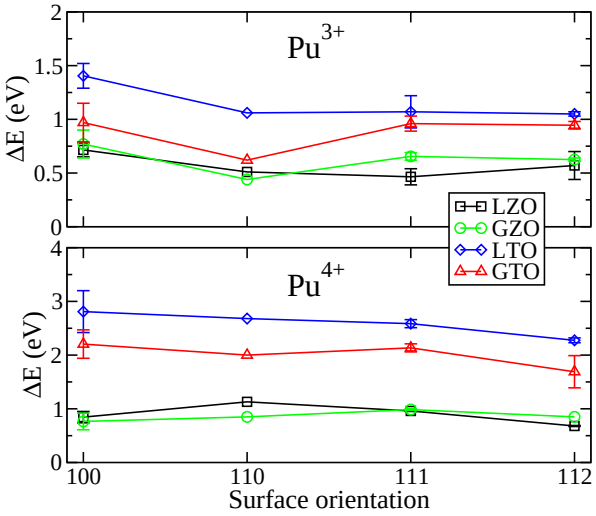

Fig. 4 Segregation energy of Pu^{3+} (top) and Pu^{4+} (bottom) at pyrochlore surfaces in GTO, GZO, LTO, and LZO.

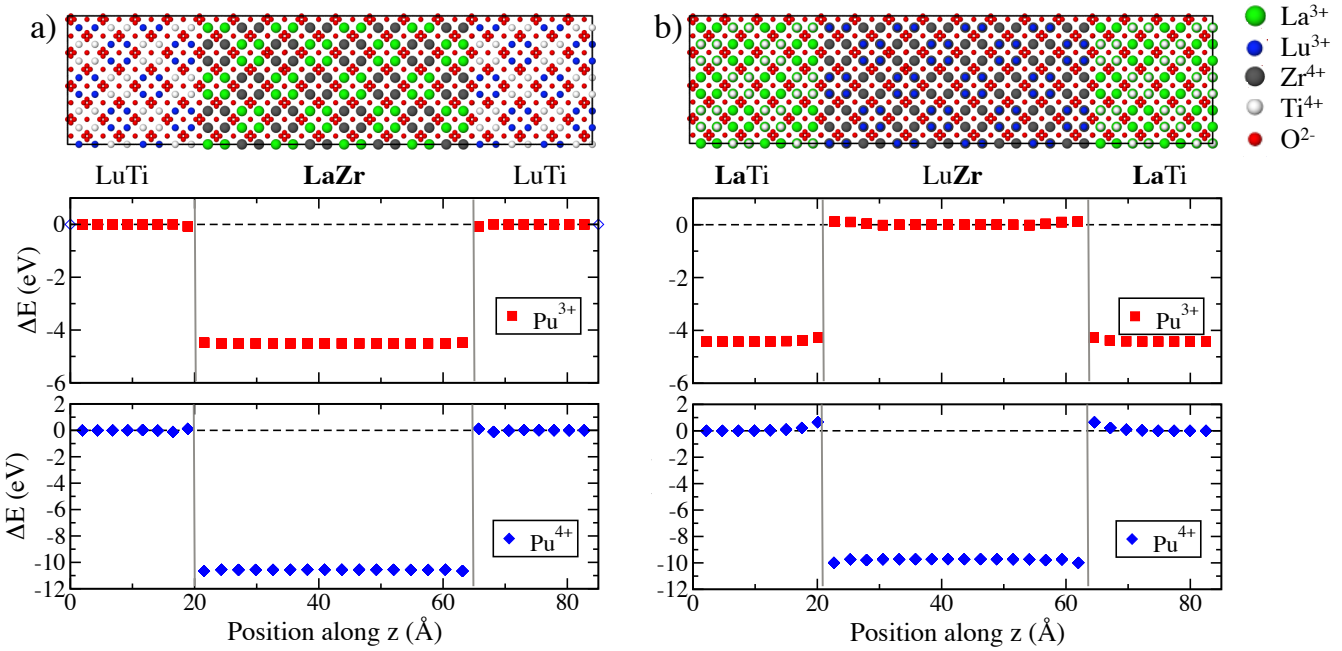

Fig. 5 Segregation of Pu in (a) LaZr/LuTi and (b) LuZr/LaTi pyrochlore bicrystals. The top panel for each compound shows the atomic structure of the bicrystal, while the middle and bottom panels are the segregation energy profiles of Pu^{3+} and Pu^{4+}, respectively, across the bicrystal structure. The zero of energy corresponds to the energy of incorporation in the bulk of the phase with the higher incorporation energy. The larger of the A/A' and B/B' cations is highlighted in bold underneath the structure. The zero of energy is taken as the incorporation energy in the bulk of the phase with the higher incorporation energy.

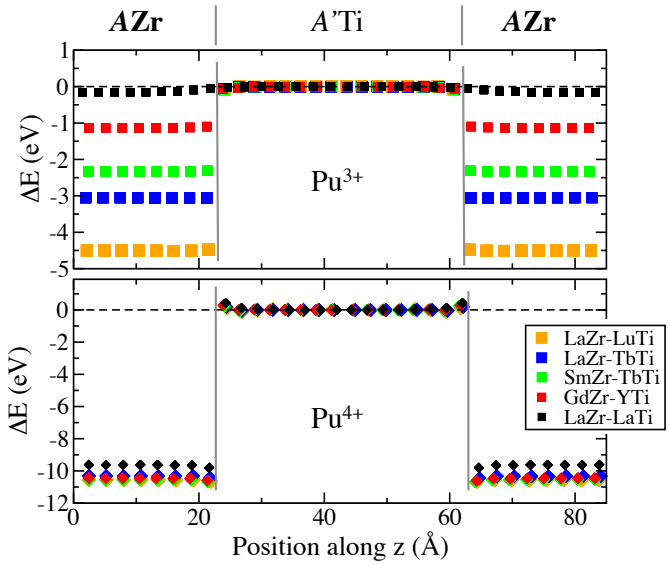

Fig. 6 Segregation energy profiles of (top) Pu^{3+} and (bottom) Pu^{4+} in AZr/A'Ti pyrochlore bicrystals for various A and A' chemistries. The compounds are listed according to increasing r_A-$r_{A'}$ ionic radii differences. The larger of the A/A' and B/B' cations is written in bold on top; in these calculations, the radius of A' is always smaller than that of A. The zero of energy is taken to be the incorporation energy in the bulk of the A'Ti phase.

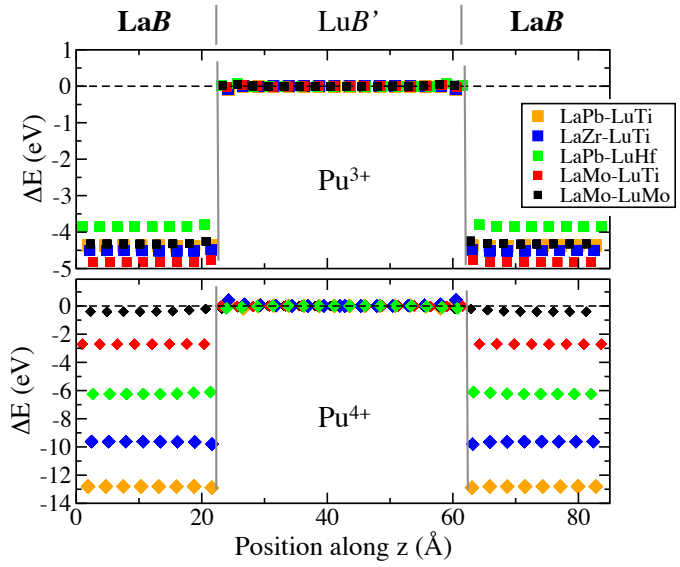

Fig. 7 Segregation energy profiles of Pu^{3+} (top) and Pu^{4+} (bottom) in LaB/LuB' pyrochlore bicrystals for various B and B' chemistries. The compounds are listed according to increasing r_B-$r_{B'}$ ionic radii difference. The larger of the A/A' and B/B' cations is written in bold on top; in these calculations, the radius of B' is always smaller than that of B. The zero of energy is taken to be the incorporation energy in the LuB' phase.

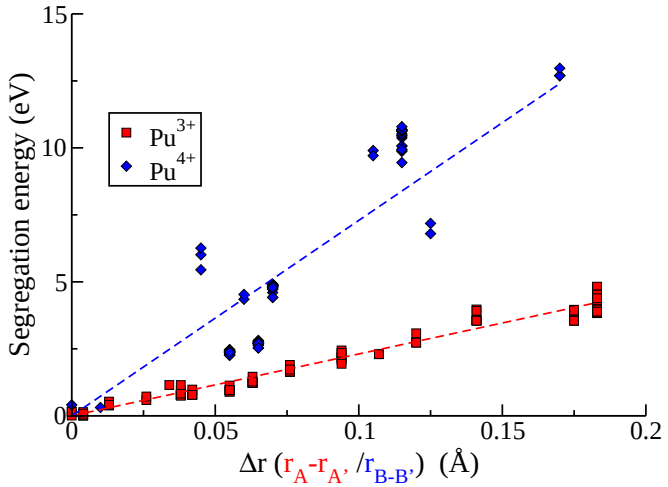

Fig. 8 Segregation energy of Pu^{3+} and Pu^{4+} to the phase containing the larger A or B cation, respectively, in pyrochlore bicrystals, as a function of r_A-$r_{A'}$ (for Pu^{3+}) and r_B-$r_{B'}$ (for Pu^{4+}). Dashed lines: linear fits to the calculated data.

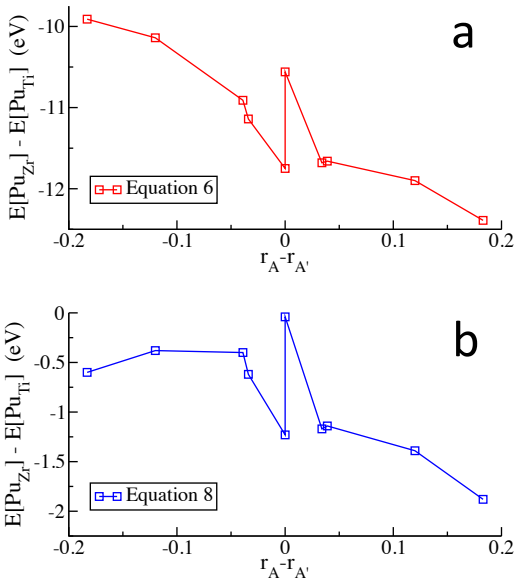

Fig. 9 Incorporation energy of Pu^{4+} in $A_2Zr_2O_7/A'_2Ti_2O_7$, calculated using Eq. 6 (a) and Eq. 8 (b).

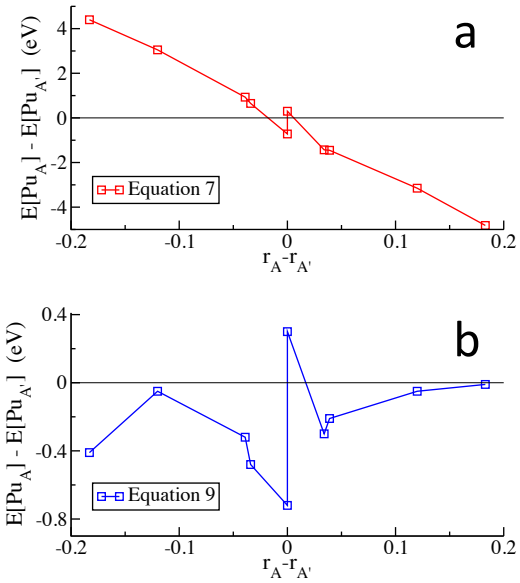

Fig. 10 Incorporation energy of Pu^{3+} in $A_2Zr_2O_7/A'_2Ti_2O_7$, calculated using Eq. 7 (a) and Eq. 9 (b).

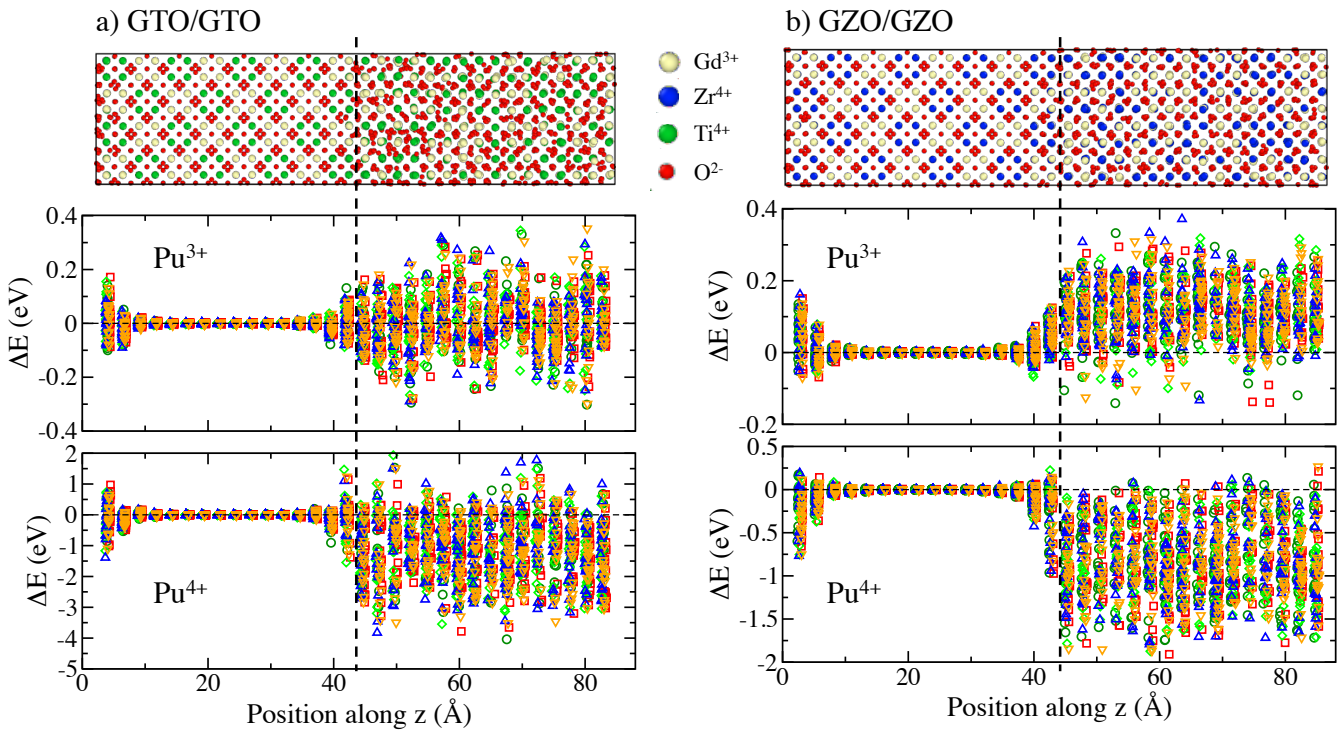

Fig. 11 Segregation of Pu in (a) GTO and (b) GZO order/disorder bicrystals. Top panel: atomic structure of the bicrystal in which the ordered phase is on the left and the disordered phase on the right of the structure. The order/disorder interface is marked by a dashed line. Middle (bottom) panel: energy of Pu^{3+} (Pu^{4+}) substitution across the bicrystal structure. Different symbols/colors represent different order/disorder structures that vary in oxygen distribution (see text).

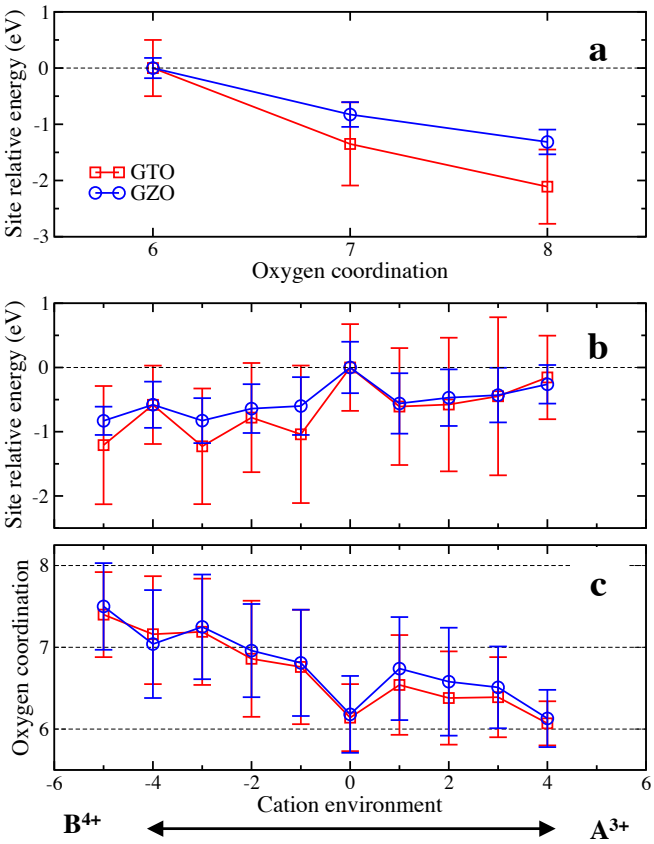

Fig. 12 Pu^{4+} substitution site energy as a function of the (a) oxygen and (b) cation environments, and (c) oxygen coordination as a function of the cation environment in the order/disorder bicrystals. The cation environment measures the deviation from the ideal arrangement or ordered pyrochlores, where each cation is surrounded by 6 A and 6 B nearest-neighbors, and essentially is a measure of whether the sites are in A rich or B rich local environments. The sharp peaks at values of zero reflect the contribution of the ordered bulk

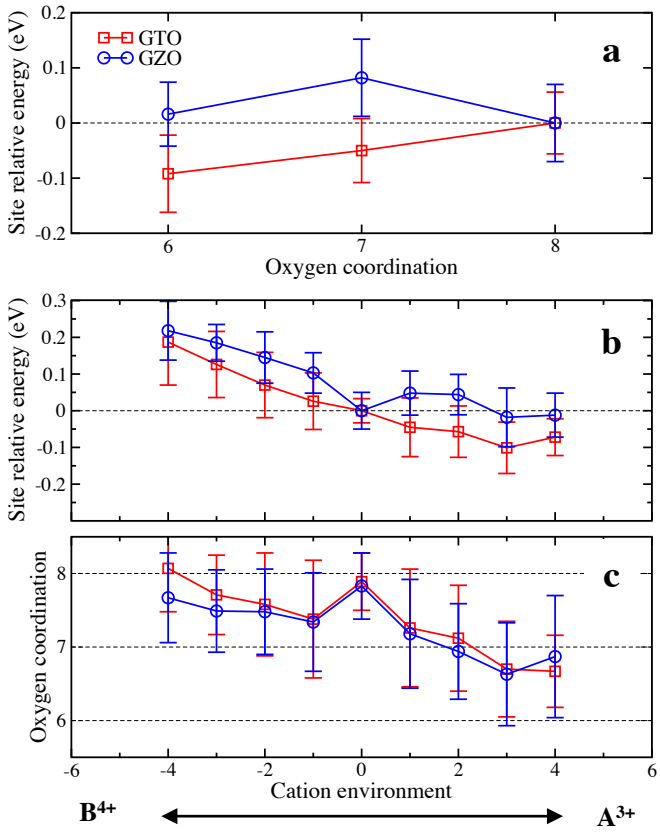

Fig. 13 Pu^{3+} substitution site energy as a function of the (a) oxygen and (b) cation environments, and (c) oxygen coordination as a function of the cation environment in the order/disorder bicrystal. As with Fig. 12, the cation environment measures the deviation from the ideal arrangement or ordered pyrochlores, where each cation is surrounded by 6 A and 6 B nearest-neighbors. The sharp peaks at values of zero reflect the contribution of the ordered bulk

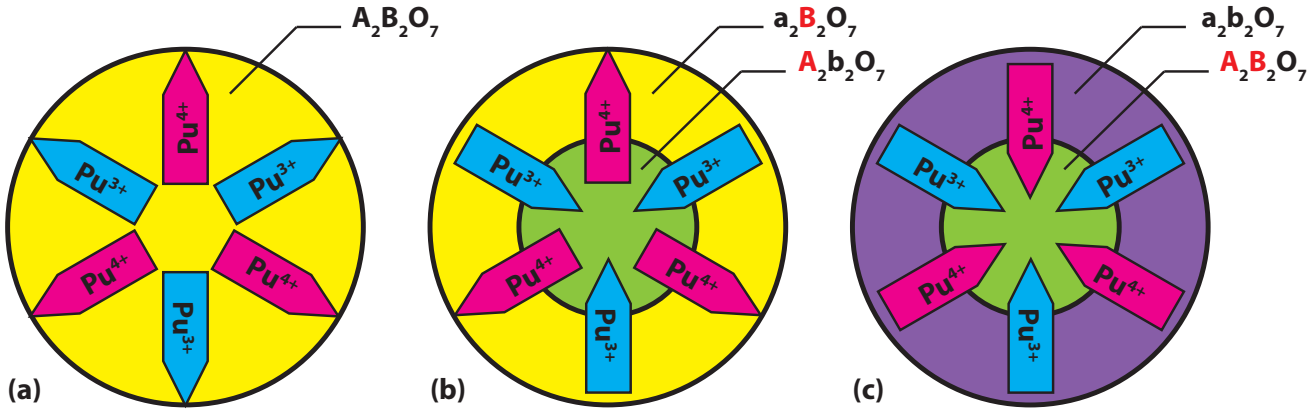

Fig. 14 Schematic illustrating the role of pyrochlore chemistry on Pu segregation in pyrochlore composites. In the chemical formulae in (b) and (c), red/uppercase denotes cation chemistries that are favorable for substitution while black/lowercase denotes chemistries that are unfavorable for substitution between the two regions. (a) In a single phase material, both Pu^{3+} and Pu^{4+} will segregate to the surface. In a composite structure, containing two different pyrochlore chemistries, (b) Pu^{3+} might segregate to one chemistry while Pu^{4+} segregates to the surface, leading to a separation of the two valence states or (c) both species might segregate to the interior phase, away from the free surface. The various combinations lead to new possibilities to tailor waste form behavior. This model assumes a closed system, and a fixed concentration of Pu

References

1 J. Bruno and R. C. Ewing, *Elements*, 2006, **2**, 343–349.

2 W. J. Weber, R. C. Ewing, C. R. A. Catlow, T. Diaz de la Rubia, L. W. Hobbs, C. Kinoshita, H. Matzke, M. Nastasi, E. Salje, E. Vance and S. Zinkle, *J. Mater. Res.*, 1998, **13**, 1434–1484.

3 B. Begg, E. Vance and S. Conradson, *J. Alloys Compd.*, 1998, **271**, 221–226.

4 E. R. Vance, G. R. Lumpkin, M. L. Carter, D. J. Cassidy, C. J. Ball, R. A. Day and B. D. Begg, *J. Am. Ceram. Soc.*, 2002, **59**, 1853–1859.

5 R. C. Ewing, W. J. Weber and J. Lian, *J. Appl. Phys.*, 2004, **5949**, 5949–5971.

6 G. R. Lumpkin, *Elements*, 2006, **2**, 365–372.

7 K. E. Sickafus, L. Minervini, R. W. Grimes, J. A. Valdez, M. Ishimaru, F. Li, K. J. McClellan and T. Hartmann, *Science*, 2000, **289**, 748–751.

8 K. E. Sickafus, R. W. Grimes, J. A. Valdez, A. Cleave, M. Tang, M. Ishimaru, S. M. Corish, C. R. Stanek and B. P. Uberuaga, *Nat. Mater.*, 2007, **6**, 217–223.

9 W. J. Weber and R. C. Ewing, *Science*, 2000, **289**, 2051–2052.

10 G. R. Lumpkin, *J. Nucl. Mater.*, 2001, **289**, 136–166.

11 A. E. Ringwood, *Mineral. Mag.*, 1985, **49**, 159–176.

12 A. E. Ringwood, S. E. Kesson, N. G. Ware, W. Hibberson and A. Major, *Nature*, 1979, **278**, 219–223.

13 G. R. Lumpkin and R. C. Ewing, in *Natural Pyrochlores: Analogues for Actinides Host Phases in Radioactive Waste Forms*, ed. J. A. S. C. M. Jantzen and R. C. Ewing, Materials Research Society Symposium Proceedings, Pittsburgh, Pennsylvania, 1985, vol. 44, pp. 647–654.

14 W. J. Weber, J. W. Wald and H. Matzke, *Mater. Lett.*, 1985, **3**, 173–180.

15 W. J. Weber, J. W. Wald and H. Matzke, *J. Nucl. Mater.*, 1986, **138**, 196–209.

16 Y. F. Volkov, S. V. Tomilin, A. N. Lukinykh, A. A. Lizin, A. A. Elesin, A. G. Yakovenko, V. I. Spiryakov, A. V. Bychkov and L. J. Jardine, *Radiochemistry*, 2004, **46**, 351–357.

17 D. M. Strachan, R. D. Scheele, E. C. Buck, J. P. Icenhower, A. E. Kozelisky, R. L. Sell, R. J. Elovich and W. C. Buchmiller, *J. Nucl. Mater.*, 2005, **345**, 109–135.

18 S. X. Wang, B. D. Begg, L. M. Wang, R. C. Ewing, W. J. Weber and K. V. Govidan Kutty, *J. Mater. Res.*, 1999, **14**, 4470–4473.

19 R. Devanathan, J. Weber and J. D. Gale, *Energy and Environmental Science*, 2010, **3**, 1551–1559.

20 S. Yamazaki, T. Yamashita and T. Matsui, *J. Nucl. Mater.*, 2001, **294**, 183–187.

21 N. K. Kulkarni, S. Sampath and V. Venugopal, *J. Nucl. Mater.*, 2000, **281**, 248–250.

22 D. J. Gregg, Y. Zhang, S. C. Middleburgh, S. D. Conradson, G. Triani, G. R. Lumpkin and E. R. Vance, *J. Nucl. Mater.*, 2013, **443**, 444–451.

23 R. E. Williford and W. J. Weber, *J. Nucl. Mater.*, 2001, **299**, 140–147.

24 A. Cleave, R. W. Grimes and K. E. Sickafus, *Phil. Mag.*, 2005, **85**, 967–980.

25 C. R. Stanek, C. Jiang, B. P. Uberuaga, K. E. Sickafus, A. R. Cleave and R. W. Grimes, *Phys. Rev. B*, 2009, **80**, 174101 1–10.

26 H. L. Tuller, *J. Phys. Chem. Solids*, 1995, **55**, 1393–1404.

27 P. K. Moon and H. L. Tuller, *Solid State Ionics*, 1988, **28-30**, 470–474.

28 B. P. Uberuaga and R. Perriot, *Phys. Chem. Chem. Phys.*, 2015, **17**, 24215–24223.

29 Y. F. Volkov, S. V. Tomilin, A. N. Lukinykh, A. A. Lizin, A. A. Elesin, A. G. Yakovenko, V. I. Spiryakov, V. I. Konovalov, V. M. Chistyakov, A. V. Bychkov and L. J. Jardine, *Radiochemistry*, 2004, **46**, 358–363.

30 N. P. Laverov, S. V. Yudintsev, V. I. Velichkin, A. N. Lukinykh, S. V. Tomilin, A. A. Lizin and S. V. Stefanovskii, *Radiochemistry*, 2009, **51**, 529–536.

31 F. A. Kröger and H. J. Vink, *Solid State Physics - Advances in Research and Applications*, Academic Press, New York, 1957.

32 S. Plimpton, *J. Comp. Phys.*, 1995, **117**, 1–19.

33 B. P. Uberuaga, R. Smith, a. R. Cleave, F. Montalenti, G. Henkelman, R. W. Grimes, a. F. Voter and K. E. Sickafus, *Physical review letters*, 2004, **92**, 115505.

34 B. P. Uberuaga, S. Choudhury, X.-M. Bai and N. A. Benedek, *Scripta Materialia*, 2012, **66**, 105–108.

35 L. Minervini, R. W. Grimes and K. E. Sickafus, *J. Am. Ceram. Soc.*, 2000, **83**, 1873–1878.

36 M. Levy, *PhD thesis*, Imperial College, London, 2005.

37 C. R. Stanek, K. J. McClellan, M. R. Levy and R. W. Grimes, *Phys. Stat. Sol. (b)*, 2006, **243**, R75–R77.

38 P. D. Dholabhai, R. Perriot and B. P. Uberuaga, *J. Phys. Chem. C*, 2016, 10485–10499.

39 R. D. Shannon, *Acta Cryst.*, 1976, **A 32**, 751–767.

40 J.-P. Crocombette and A. Chartier, *Nuclear Instruments and Methods in Physics Research Section B: Beam Interactions with Materials and Atoms*, 2007, **255**, 158–165.

41 G. R. Lumpkin, M. Pruneda, S. Rios, K. L. Smith, K. Trachenko, K. R. Whittle and N. J. Zaluzec, *J. Solid State Chem.*, 2007, **180**, 1512–1518.

42 K. R. Whittle, M. G. Blackford, R. D. Aughterson, G. R. Lumpkin and N. J. Zaluzec, *Acta Mater.*, 2011, **59**, 7530–7537.

43 R. Perriot and B. P. Uberuaga, *J. Mater. Chem. A*, 2015, **3**, 11554–11565.

44 J. Shamblin, M. Feygenson, J. Neuefeind, C. L. Tracy, F. Zhang, S. Finkeldei, D. Bosbach, H. Zhou, R. C. Ewing and M. Lang, *Nature Materials*, 2016, **15**, 507–512.

45 C. Jiang, C. R. Stanek, K. E. Sickafus and B. P. Uberuaga, *Phys. Rev. B*, 2009, **79**, 104203 1–5.

46 Y. Li, P. M. Kowalski, G. Beridze, A. R. Birnie, S. Finkeldei and D. Bosbach, *Scripta Mater.*, 2015, **15**, 18–21.

47 M. M. Hasan, P. D. Dholabhai, R. H. R. Castro and B. P. Uberuaga, *Surf. Sci.*, 2016, **649**, 138–145.

48 C. R. Stanek, M. R. Bradford and R. W. Grimes, *J. Phys.: Condens. Matter*, 2004, **16**, S2699–S2714.

49 T. X. T. Sayle, S. C. Parker and C. R. A. Catlow, *J. Phys. Chem.*,

1994, **98**, 13625–13630.
50 B. Slater, C. R. A. Catlow, D. H. Gay, D. E. Williams and V. Dusastre, *J. Phys. Chem.*, 1999, **2**, 10644–10650.
51 P. R. Kenway, P. M. Oliver, S. C. Parker, D. C. Sayle, T. X. T. Sayle and J. O. Titiloye, *Mol. Simul.*, 1992, **9**, 83–98.
52 E. A. Colbourn, W. C. MacKrodt and P. W. Tasker, *J. Mater. Sci.*, 1983, **18**, 1917–1924.
53 R. C. Mccune and P. Wynblatt, *J. Am. Ceram. Soc.*, 1982, **66**, 111–117.
54 S. Baik and C. L. White, *J. Am. Ceram. Soc.*, 1987, **70**, 682–688.
55 M. J. Davies, P. R. Kenway, P. J. Lawrence, S. C. Parker, W. C. Mackrodt and P. W. Tasker, *J. Chem. Soc., Faraday Trans. 2*, 1989, **85**, 555–563.
56 P. J. Lawrence, S. C. Parker and P. W. Tasker, *J. Am. Ceram. Soc.*, 1988, **71**, 389–391.
57 G. R. Lumpkin and R. C. Ewing, *Phys. Chem. Minerals*, 1988, **16**, 2–20.
58 R. C. Ewing, W. J. Weber and F. W. Clinard, *Progress in Nuclear Energy*, 1995, **29**, 63–127.
59 P. P. Dholabhai, J. A. Aguiar, A. Misra and B. P. Uberuaga, *J. Chem. Phys.*, 2014, **140**, 194701 1–12.
60 S. Finkeldei, F. Brandt, K. Rozov, A. A. Bukaemskiy, S. Neumeier and D. Bosbach, *Appl. Geochem.*, 2014, **49**, 31–41.
61 A. Zunger, S. H. Wei, L. G. Ferreira and J. E. Bernard, *Phys. Rev. Lett.*, 1990, **65**, 353–356.
62 J. A. Valdez, I. O. Usov, J. Won, M. Tang, R. M. Dickerson, G. D. Jarvinen and K. E. Sickafus, *J. Nucl. Mater.*, 2009, **393**, 126–133.
63 X. Y. Liu, B. P. Uberuaga, P. Nerikar, C. R. Stanek and K. E. Sickafus, *Nucl. Instrum. Methods Phys. Res. Sec. B*, 2010, **268**, 3014–3017.
64 B. P. Uberuaga, S. Choudhury and A. Caro, *J. Nucl. Mater.*, 2014, **462**, 402–408.
65 I. J. Beyerlein, M. J. Demkowicz, A. Misra and B. P. Uberuaga, *Prog. Mater. Sci.*, 2015, **74**, 125–210.